Keynote Paper

Design Tools for Digital Microfluidic Biochips: Toward Functional Diversification and More than Moore

Krishnendu Chakrabarty, *Fellow, IEEE,* Richard B. Fair, *Life Fellow, IEEE,* and Jun Zeng, *Member, IEEE*

***Abstract*—Microfluidics-based biochips enable the precise control of nanoliter volumes of biochemical samples and reagents. They combine electronics with biology, and they integrate various bioassay operations, such as sample preparation, analysis, separation, and detection. Compared to conventional laboratory procedures, which are cumbersome and expensive, miniaturized biochips offer the advantages of higher sensitivity, lower cost due to smaller sample and reagent volumes, system integration, and less likelihood of human error. This paper first describes the droplet-based "digital" microfluidic technology platform and emerging applications. The physical principles underlying droplet actuation are next described. Finally, the paper presents computer-aided design tools for simulation, synthesis and chip optimization. These tools target modeling and simulation, scheduling, module placement, droplet routing, pin-constrained chip design, and testing.**

***Index Terms*—Clinical diagnostics, lab-on-chip, simulation, synthesis, testing.**

I. Introduction

ADVANCES in digital microfluidics have led to the promise of miniaturized biochips for applications such as immunoassays for point-of-care medical diagnostics, deoxyribonucleic acid (DNA) sequencing, and the detection of airborne particulate matter [1]–[8]. These devices enable the precise control of nanoliter droplets of biochemical samples and reagents, and integrated circuit (IC) technology can be used to transport and process "biochemical payload" in the form of tiny droplets. Biochips facilitate the convergence of electronics with the life sciences, and they integrate on-chip various bioassay operations, such as sample preparation, analysis, separation, and detection [1], [4]. Compared to conventional laboratory procedures, which are cumbersome and expensive, miniaturized biochips offer the advantages of higher sensitivity, lower cost due to smaller sample and reagent volumes, higher levels of system integration, and less likelihood of human error. As a result, non-traditional biomedical applications and markets are opening up fundamentally new uses for ICs.

However, continued growth in this emerging field depends on advances in chip/system integration. In particular, design methods are needed to ensure that biochips are as versatile as the macro-labs that they are intended to replace. The few commercial biochips available today (e.g., from Agilent, Fluidigm, Caliper, I-Stat, BioSite, etc.) are specific to certain applications, e.g., electrophoresis, and they offer no flexibility to the user. Design challenges for digital microfluidics include scheduling and binding of fluidic operations, placement of modules, and droplet routing. Typical design objectives include small chip area, reduced assay completion time, and ease of droplet routing. Defect tolerance is also important, especially for disease screening, food-safety tests, and pharmacological procedures that require high precision.

This tutorial paper is focused on droplet-based "digital" microfluidic biochips. The digital microfluidics platform offers the flexibility of dynamic reconfigurability and software-based control of multifunctional biochips. The paper describes emerging computer-aided design (CAD) tools for the automated synthesis and optimization of biochips from bioassay protocols. The physical principles underlying droplet movement are explained. Recent advances in modeling and simulation, fluidic-operation scheduling, module placement, droplet routing, testing, and dynamic reconfiguration are also presented. These CAD techniques allow biochip users to concentrate on the development of nanoscale bioassays, leaving chip optimization and implementation details to design-automation tools.

It is expected that an automated design flow will transform biochip research and use, in the same way as design automation revolutionized IC design in the 1980s and 1990s. This approach is therefore especially aligned with the vision of functional diversification and "More than Moore," as articulated in the International Technology Roadmap for Semiconductors 2007, which highlights "Medical" as being a "System Driver" for the future [9]. Biochip users will adapt more easily to emerging technology if appropriate design methods/tools and

Manuscript received October 19, 2009; revised March 1 2010. Date of current version June 18, 2010. This work was supported in part by the U.S. National Science Foundation, under Grants IIS-0312352, CCF-0541055, and CCF-0914895, and the National Institute of General Medical Sciences of the National Institute of Health, under Grant R44GM072155. This paper was recommended by Associate Editor V. Narayanan.

K. Chakrabarty and R. B. Fair are with the Department of Electrical and Computer Engineering, Duke University, Durham, NC 27708 USA (e-mail: krish@ee.duke.edu; rfair@ee.duke.edu).

J. Zeng is with Hewlett-Packard Laboratories, Hewlett-Packard Company, Palo Alto, CA 94304 USA (e-mail: jun.zeng@hp.com).

Color versions of one or more of the figures in this paper are available online at http://ieeexplore.ieee.org.

Digital Object Identifier 10.1109/TCAD.2010.2049153

in-system automation methods are available. CAD techniques for microfluidic biochips must adequately handle unique constraints that arise due to the fluidic aspects of the underlying technology, the likelihood of cross-contamination between different bio-molecules, and the limited availability of stock solutions for use in assay protocols in biochemistry.

The rest of this paper is organized as follows. Section II describes biochip technology platforms, including digital microfluidics, and outlines some emerging applications. Sections III and IV describe the physics of droplet actuation, and present modeling and simulation methods. Section V presents synthesis techniques, including solutions published in the literature for operation scheduling, module placement, and droplet routing. Section VI describes pin-constrained chip methods. Section VII presents advances in testing, diagnosis, and dynamic reconfiguration. Finally, Section VIII concludes the paper.

II. Technology Platforms and Applications

Early biochips were based on the concept of a DNA microarray, which is a piece of glass, plastic or silicon substrate on which pieces of DNA, i.e., probes, have been affixed. There are a number of commercial microarrays available in the marketplace today, e.g., GeneChip DNAarray from Affymetrix, NanoChip microarray from Nanogen, and DNA microarray from Agilent. A drawback of these arrays is that they are "passive chips;" they are neither reconfigurable nor can they be used for sample preparation.

The basic idea of a microfluidic biochip is to integrate all necessary functions for biochemical analysis using microfluidics technology. These micro-total-analysis-systems are more versatile than microarrays. Integrated functions include assay operations, detection, and sample preparation.

A. Continuous-Flow Microfluidics

Traditional (continuous-flow) microfluidic technologies are based on the continuous flow of liquid through microfabricated channels [16], [18]–[23]. Continuous-flow systems are inherently difficult to integrate because the parameters that govern flow field (e.g., pressure, fluid resistance, electric field strength) vary along the flow-path, making the flow at any location dependent upon the properties of the entire system. Moreover, unavoidable shear flow and diffusion in microchannels make it difficult to eliminate intersample contamination and dead volumes. Furthermore, since structure and functionality are so tightly coupled, each system is only appropriate for a narrow class of applications.

B. Digital Microfluidics

The concept of digital microfluidics arose in the late 1990s and involves the manipulation of discrete volumes of liquids on a surface. Manipulation of droplets can occur through various mechanisms, including electrowetting [10]–[12], dielectrophoresis [13], thermocapillary transport [14], and surface acoustic wave transport [15]. In the digital microfluidic architecture the basic liquid unit volume is fixed

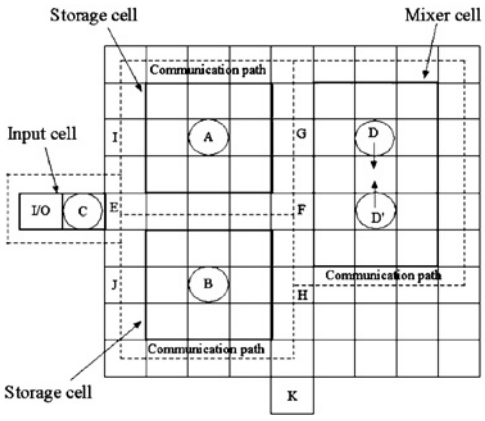

Fig. 1. 2-D electrowetting electrode array used in digital microfluidic architecture [17].

by the geometry of the system (fluid quantization), whereas volumetric flow rate is determined by the droplet transport rate and the number of droplets transported. Thus, transport occurs in multiples of the minimum unit volume (fluid packetization). Unlike continuous-flow systems, the minimum flow volume in a digital microfluidic system is not determined by the sensitivity of a flow sensor, since there is no flow sensor. Rather, minimum droplet volume is set by detector sensitivity [16].

The use of unit volume droplets allows a microfluidic function to be reduced to a set of basic operations, allowing numerous elemental fluidic operations to be accomplished with a common set of elemental components, i.e., combinations of electrodes on an array [19]. An example of the digital microfluidic architecture is shown in Fig. 1. Depicted is a 2-D array of electrodes configured for an electrowetting-on-dielectric (EWD) system [17].

EWD microfluidics is based on the actuation of droplet volumes up to several microliters using the principle of modulating the interfacial tension between a liquid and an electrode coated with a dielectric layer [18]. An electric field established in the dielectric layer creates an imbalance of interfacial tension if the electric field is applied to only one portion of the droplet on an array, which forces the droplet to move [10]. The architecture of Fig. 1 capitalizes on the flexibility of a unit flow grid array. At any given time, the array can be partitioned into "cells" that perform fluidic functions, such as storage, mixing, or transport. If the array is actuated by a clock that can change the voltage at each electrode on the array in one clock cycle, then the architecture has the potential for dynamically reconfiguring the functional cells at least once per clock cycle. Thus, once the fluidic function defined by a cell is completed, the cell electrode voltages can be reconfigured for the next function.

The digital microfluidic architecture is characterized by software-driven electronic control, eliminating the need for mechanical tubes, pumps, and valves that are required for continuous-flow systems. The compatibility of each chemical substance with the electrowetting platform must be determined initially. The following compatibility issues must be considered: 1) does the liquid's viscosity and surface tension allow for droplet dispensing and transport by electrowetting? 2) Will the contents of the droplet foul the hydrophobic surfaces of

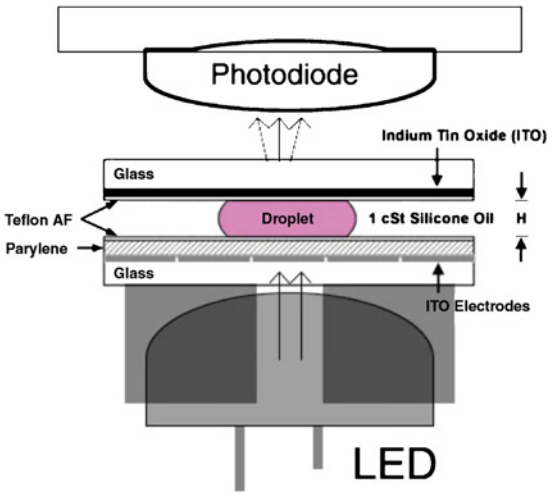

Fig. 2. Optical absorbance measurement instrumentation used to monitor color change due to colorimetric reactions on chip.

the chip? 3) In systems with a silicone oil medium, will the chemicals in the droplet cross the droplet/oil interface, thus reducing the content in the droplet? and 4) What type of detection method is suitable? Next, we describe some typical applications of digital microfluidics.

C. Colorimetric Assays

On-chip colorimetric assays for determining the concentrations of target analytes is a natural application for digital microfluidics [2], [20], [21]. The specific focus of work in this area has been on multiplexed assays, where multiple analytes can be measured in a single sample. The on-chip process steps include the following: 1) pre-diluted sample and reagent loading into on-chip reservoirs; 2) droplet dispensing of analyte solutions and reagents; 3) droplet transport; and 4) mixing of analyte solutions. Srinivasan *et al.*, have demonstrated a colorimetric enzyme-kinetic method based on the Trinder's reaction used for the determination of glucose concentration. This reaction is based on enzymes that oxidize glucose to form a violet colored compound [7]. At the end of the mixing phase, the absorbance is measured for at least 30 s, using a 545 nm light-emitting diode-photodiode setup. The mixed droplet is held stationary by electrowetting forces during the absorbance measurement step, depicted in Fig. 2.

The integration of optical sources and detectors based on absorbance is relatively easy to perform on a digital microfluidic platform, especially since the platform is made using plates and see-through indium-tin-oxide electrodes. However, optical absorbtion detection scales poorly with miniaturization, since Beer's law incorporates a pathlength dependence [22]. Regarding the detectors reported by Srinivasan *et al.* the optical path length typically was 100–300 μm [20], which is 30–100 times smaller than conventional systems (10 mm). This small path length poses serious sensitivity issues, and limits the use of absorbance to assays with very high analyte concentrations.

D. Chemiluminescent Assays

Chemiluminescence detection has been shown to be compatible with the digital microfluidic platform and with diagnostic

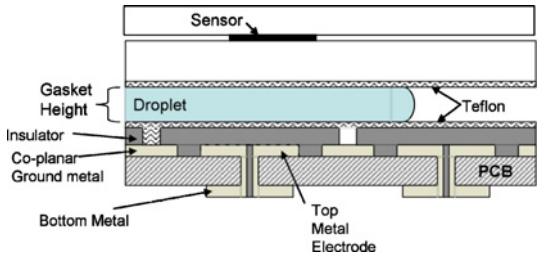

Fig. 3. Side view of a co-planar electrowetting chip made on a PCB. The top plate can be customized.

applications as well as sequencing DNA by synthesis [23]. In general, the on-chip chemistry must result in optical signal generation in the vicinity of a photodetector. Work in this area has been reported by Luan *et al.* with an integrated optical sensor based upon the heterogeneous integration of an InGaAs-based thin film photodetector with a digital microfluidic system [24].

To integrate a compound semiconductor photodetector with an electrowetting microfluidics system, a co-planar digital microfluidic chip fabricated by the Advanced Liquid Logic in printed circuit board (PCB) technology, was used. The chip was attached to the controller, and electrodes were switched through a computer graphic user interface connected to the controller. Silicone oil ($\sim$2 cSt) was dispensed onto the area of the chip used for this experiment. Electrode voltages of 220-V were applied to the chip. A side view of the integrated sensor is shown in Fig. 3 [24].

In order to generate a substantial signal in an aqueous medium, the oxidation of pyrogallol (1,2,3-trihydroxibenzene) in an alkaline solution was used (the Trautz–Schorigin reaction). When two droplets are mixed it generates a short-lived, bright orange light if the solution is fresh, or a longer lasting, lower intensity light if the solution is not fresh (has been given time to cool). Both solutions are immiscible in silicone oil. Chemicals used in the experiments were dispensed from on-chip reservoirs, and the dispensed droplets were actuated together underneath the sensor. When the droplets mixed underneath the sensor, the chemiluminescent reaction began to generate light.

Another example of chemilumescent detection is DNA sequencing by synthesis. Sequencing-by-synthesis methods involve enzymatic extension by polymerase through the iterative addition of labeled nucleotides, often in an array format. The cascade begins with the addition of a known nucleotide to the DNA (or ribonucleic acid) strand of interest. This reaction is carried out by DNA polymerase. Upon nucleotide incorporation, pyrophosphate (PPi) is released. This pyrophosphate is converted to ATP by the enzyme ATP sulfurylase. The ATP then provides energy for the enzyme lucerifase to oxidize luciferin. One of the byproducts of this final oxidation reaction is light at approximately 560 nm. This sequence is shown in Fig. 4.

The light can be easily detected by a photodiode, photomultiplier tube, or a charge-coupled device (CCD). Since the order in which the nucleotide addition occurs is known, one can determine the sequence of the unknown strand by formation of

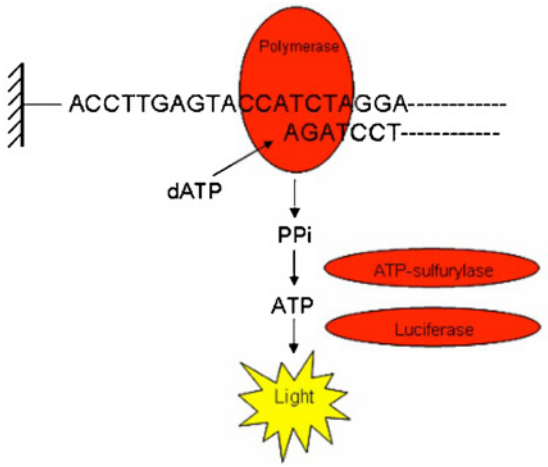

Fig. 4. Illustration of solid-phase pyrosequencing. After incorporation of a nucleotide (in this case dATP), a washing step is used to remove the excess substrate.

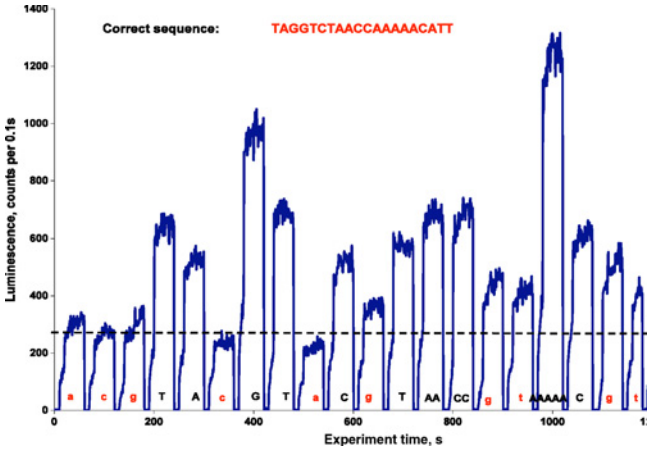

Fig. 5. On-chip pyrosequencing results showing 17-bp sequencing of a 211-bp long *C. albicans* DNA template.

its complimentary strand. The entire pyrosequencing cascade takes about 3–4 s from start to finish per nucleotide added.

Pyrosequencing of DNA has been performed on a digital microfluidic platform [23]. The chip was covered with a transparent top plate and filled with oil to create a microfluidic chamber in which droplets were programmably manipulated (dispensed, transported, merged, and split) using electrical fields. Using a 211 bp DNA fragment derived from *C. albicans* genomic DNA, single stranded templates were prepared and attached to 2.8 μm magnetic beads.

The bead suspension and pyrosequencing reagents were loaded in wells formed in the top-plate. Unit-sized 400 nL droplets were dispensed from the wells and manipulated within the chip according to the user program. At each cycle the sample droplet containing the beads was combined with one droplet containing nucleotides and one droplet containing the three-enzyme mixture. The combined droplet was mixed and transported to a detector where a luminescent signal proportional to the number of bases incorporated was detected by a photomultiplier coupled to the transparent top plate. The combined droplet was then transported to a wash station with a permanent magnet located underneath the chip. Washing was performed by repeated addition and removal of fresh buffer droplets to the sample droplet while the magnetic beads were immobilized on the chip surface. The entire cycle was then repeated with a fresh enzyme droplet and a fresh nucleotide droplet selected from one of the four nucleotide wells. Up to 20 bases in three different regions of the 211 bp template were successfully sequenced using this technique. Results of a 20 bp read are shown in Fig. 5 [23].

E. High Sensitivity Integrated Sensors

To expand the applications of digital microfluidics to new areas requires integration of sensing systems that are sensitive enough to detect latent and subclinical infections. As an example, the input to the digital microfluidic platform would be a drop of blood. The blood is then processed by the microfluidic system to separate the red blood cells containing the parasite, the cells are lysed, and the DNA is extracted from the contents of the cell (including the parasite). The microfluidic system for this application contains stabilized reagents that are then used to isolate the targeted DNA strands, and to "unzip" the DNA, resulting in single strand DNA that is the target DNA. The DNA is then amplified using polymerase chain reaction (PCR) or isothermal amplification, and then is presented to the integrated optical sensor. The amplification step time will be minimized through the use of a high sensitivity optical sensor and amplification at the sensing surface. The optical sensors are surface customized with the single strand DNA (the "probe") that is complementary to the target [25].

III. Physics of Droplets

In this section, we describe the physical principles underlying droplet motion. An understanding of the physics of droplets is necessary for accurate modeling and simulation.

A. Forces in Play and Actuation Methods

Microfluidics research is witnessing a paradigm shift from the continuous-flow-based architecture to the droplet-based architecture, in particular, the digital microfluidics. Using droplets as "chemical processing plants" has operational benefits in addition to the architectural advantages mentioned in previous sections. The larger surface-to-volume ratio and flow circulation within the droplet provide efficient mixing and thermal dissipation, and enable shorter reaction times. Each droplet is an independent reactor; it compartmentalizes sample species, eliminating the issues associated with Taylor–Aris dispersion [79] that has been detrimental for continuous-flow-based architecture.

With digital microfluidics, complex procedures are built up through combining and reusing a finite set of basic instructions including droplet generation, droplet translocation, droplet fusion, and droplet fission. Hydrodynamic forces generated by diverse actuation methods have been exploited to accomplish this set of operations.

It is commonly recognized that the first systematic scientific study of droplets was Savart's report on drop breakup mechanism in 1833. Rayleigh's work on interfacial stability analysis

in 1879 provided the theoretical foundation for the discoveries of droplet physics continuing as recent as 1970s. While theoretical works have provided qualitative understanding of many interfacial phenomena, the quantitative prediction and analysis of droplet dynamics is still an active research field relying on modeling and numerical simulation techniques.

The continuum assumption holds for microfluidics [26]. Excluding a few exceptions (e.g., piezoelectric inkjet), the compressibility of the operating liquid can be considered effectively zero. The Navier–Stokes equations thus can be applied to govern the hydrodynamics of both the droplets and the continuous phase

$$\rho\left(\frac{\partial \boldsymbol{u}}{\partial t}+(\boldsymbol{u}\cdot\nabla)\boldsymbol{u}\right)=-\nabla p+\mu\nabla^2\boldsymbol{u}+\boldsymbol{f} \tag{1}$$

where ρ is the fluid density, μ is the viscosity, $\boldsymbol{u}$ is the fluid velocity field (a divergence-free vector field due to the incompressibility assumption), p is the pressure, and $\boldsymbol{f}$ is the body force density, for instance, of electric origin. Interfacial stress balance is preserved at the interface between a droplet and the continuous phase [27]

$$\begin{aligned}(\boldsymbol{\tau}_d-\boldsymbol{\tau}_a)\cdot\boldsymbol{n}\cdot\boldsymbol{t}-\nabla y\cdot\boldsymbol{t}&=\boldsymbol{0}\\(p_d-p_a)-\gamma\nabla\cdot\boldsymbol{n}&=\boldsymbol{0}\end{aligned} \tag{2}$$

where $\boldsymbol{n}$ is the unit normal of the interface pointing out of the droplet, $\boldsymbol{t}$ is a tangential vector of unit length at the interface, p is the hydrodynamic pressure, $\boldsymbol{\tau}$ is the deviatoric stress tensor, and γ is the interfacial tension coefficient. The subscript d denotes the properties of the droplet, and the subscript a denotes the properties of the ambient continuous phase. In the cases that the droplet is in contact with a solid surface, the interaction among molecules of the three phases (droplet, the continuous phase, and the solid) leads to a net force of attraction (wetting) or repulsion (non-wetting). This force, the wetting force, denoted $\boldsymbol{f}^W$, is a line force density defined by the following expression:

$$\boldsymbol{f}^W=\gamma\cos\theta \tag{3}$$

where θ is the contact angle at the tri-phase contact line measured within the droplet between the two-fluid interface and the solid surface. $\boldsymbol{f}^W$ acts on the tri-phase contact line, and is in plane with the solid surface, perpendicular to the tri-phase contact line, and points away from the droplet.

Equations (1)–(3) unveil several possible knobs for droplet manipulation. Due to droplets' large surface-to-volume ratio, the forces (or moments) proportional to droplet volume usually are less effective comparing to forces acting on the droplet surface and/or on the tri-phase contact line. Net surface or wetting forces can be achieved through creating non-uniform distribution of γ, θ or surface pressure p_d. Below are a few practical examples.

1) Utilizing the thermal Marangoni effect that the gradients of the interfacial tension can be induced by heat transfer [28], a temperature gradient can be established along the droplet surface to achieve non-uniformly distributed surface tension γ. Such surface tension gradient results in a net surface force that can be used for droplet manipulation. An array of embedded microheaters [29] or laser heating [30] can be used to establish and modulate the temperature gradients thus the net surface force.
2) Non-uniform distribution of surface pressure can also result in a net surface force. The flow rate of the continuous phase and the channel geometry (e.g., T-channel [31]) are used to control the hydrodynamic pressure exerted on the droplet surface to achieve desired droplet breakup.
3) Magnetic field can be used for droplet manipulation. Superparamagnetic particles can be injected inside a droplet. An on-chip magnetic field can guide the movement of the particles to impact particular area of the droplet surface to achieve desired droplet movement or deformation [32].
4) The use of the electric field to carry out on-chip droplet operation is largely based upon either dielectrophoresis [33] or electrowetting on dielectric (EWD) [10] operating principles. The discontinuity of the electrical properties of the media (droplet, the continuous phase, and the solid) at the droplet surface and/or the tri-phase contact line gives rise to a significant and highly controllable surface and/or wetting forces. Digital microfluidics systems based on EWD has been developed furthest in terms of demonstrating on-chip applications that are clinically relevant [34].

B. Droplet Electrohydrodynamics and EWD

Since the inception of microfluidics, the electric force has been exploited as one of the leading mechanisms for driving and controlling the movement of operating fluid and charged suspensions. The electric force has an intrinsic advantage in miniaturized devices. Because the electrodes are placed cross a small distance, from sub-micrometer to a few micrometers, a very high electric field, order of MV/m, is rather easy to obtain. In addition, the electric force can be highly localized force, with its strength rapidly decaying moving away from the peak. This makes the electric force an ideal candidate for spatial precision control. The geometry and placement of the electrodes can be used to design electric fields of varying distributions, which can be readily realized by MEMS fabrication methods. Electric control also possesses advantages in system integration and reliability. For instance, there are no mechanical moving parts, and the system can be directly controlled through software.

When exposed to an external electric field, the free charges will migrate due to the Coulomb force. The charges bound in molecules, both the molecules of the carrier liquid and of the biochemical species, will undergo distortion of the molecular charge density, or polarize. The volumetric force density of electric origin can be expressed as [35]

$$\boldsymbol{f}^e=\rho_e\boldsymbol{E}-\sum_{i=1}^{m}\alpha_i\nabla\left(\frac{\partial W}{\partial\alpha_i}\right) \tag{4}$$

where $\boldsymbol{E}$ is the electric field, ρ_{e} the volumetric density of the free charge, W the volumetric density of the electroquasistatic energy, and $\alpha_1, \alpha_2, \ldots, \alpha_m$ the material properties. The first term is the Coulomb force density originating from free

charges. The second is the dielectrophoresis force density originating from the bounded (paired) charges. It should be noted that this volumetric force density expression is rather a convenient mathematical notation to describe this electrohydrodynamic impact, it does not indicate that such impact be a body force. In fact, later discussion will show, for instance, this volumetric force density expression under a EWD setup gives rise to a wetting force.

Microfluidics typically operates at a small length scale (less than 1 mm) and low frequency ($\ll$1 GHz). Under this circumstance, the electromagnetic wave propagation can be neglected since the characteristic dimension of the device is much smaller than the electromagnetic wavelength. This leads to the well known electroquasistatic assumption to Maxwell's equations [36] where the charge distribution exerts its effect instantly in space. The truncated version of Maxwell's equations under the electroquasistatic assumption, Poisson equation, can be applied to solve the electric field

$$\nabla^2\phi = -\frac{\rho_e}{\varepsilon} \tag{5}$$

where ϕ is the electric potential, $\boldsymbol{E} = -\nabla\phi$, and ε is the electric permittivity of the medium. The coupling between the hydrodynamics and electric field is bi-directional. The presence of the electric field adds an additional force density while simultaneously the movement of material (e.g., fluids, charged or polarizable particles) alters the electrical property distribution ε and free charge distribution ρ_e—both are functions of space—hence the electric field.

In most electrically controlled digital microfluidics platforms, droplets, the continuous phase and contacting solid phase possess different electric properties. This results in the discontinuity of the electric field intensity at the material boundaries (e.g., the droplet surface and the tri-phase contact line), which in turn results in gradient of the electrostatic energy thus gives rise of hydrodynamic forces of electric origin.

The droplets are either conductive (e.g., containing free ions or charge-carrying reverse micelles) or highly polarizable [37] (e.g., aqueous-based). At the droplet surface

$$\begin{aligned} &\boldsymbol{n}\cdot(-\varepsilon_{a,i}\nabla\phi_{a,i}) = \sigma \\ &\frac{\partial\sigma}{\partial t} + \nabla_\Sigma\cdot\sigma\boldsymbol{v} + \boldsymbol{n}\cdot k\nabla\phi_d = 0 \end{aligned} \tag{6}$$

where σ is the surface charge density at the droplet surface, κ is droplet conductivity, $\boldsymbol{v}$ is the fluid velocity inside the droplet, ∇_Σ is the interfacial divergence, and subscripts d, a, and i refer to the droplets, the continuous phase, and the contacting solid phase.

Fig. 6 illustrates a simplified EWD setup. Droplets are placed onto a thin insulating layer preventing the droplets from direct contact with the electrodes. The droplets are surrounded by an immiscible continuous phase to prevent mass loss due to evaporation. Because the droplet usually is more polar than the continuous phase, the volumetric density of the electrostatic energy stored in the portion of the thin insulating layer directly under the droplet is much higher than that stored in the thin insulating layer directly under the continuous phase. An abrupt change of the electrostatic energy occurs right underneath the tri-phase contact line which produces an electric force that acts on the contact line and induces contact angle reduction, referred to as the EWD force. When neglecting the fluid motion, this EWD force can be derived analytically according to (4), (5), and the boundary condition (6) [35]

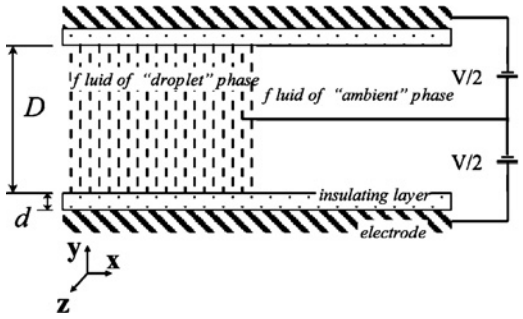

Fig. 6. Simplified EWD device.

$$\boldsymbol{f} = \frac{\varepsilon_i V^2}{8d}\left(1 - \exp\left(\frac{2d}{D}\frac{\kappa}{\varepsilon_i}t\right)\right)^2 \tag{7}$$

where V is the applied voltage, D represents droplet dimension, d is the thickness of the insulating layer, and t is the time. This EWD force acts on the tri-phase contact line and causes the reduction of the contact angle that may be described as

$$\Delta\theta = \theta_0 - a\cos(\cos\theta_0 + \boldsymbol{f}) \tag{8}$$

where θ_0 is the contact angle measured when the electric field is absent, and $\Delta\theta$ is the magnitude of the contact angle reduction due to EWD. Since $\Delta\theta$ is measurable experimentally, it is commonly used to describe the effect and the strength of EWD.

Equation (7) indicates that, after a transient period defined by the time constant $\tau_e = (D/2d)(\varepsilon_i/\kappa)$, the EWD force approaches to its maximum, which is the EWD force expression commonly cited in literature. When the droplet is reasonably conductive (e.g., 55 mS/m as cell cultures diluted with an isotonic buffer), and not too small (e.g., order of 100 μm), $\boldsymbol{\tau}_e$ is small compared to the hydrodynamic time constant $\boldsymbol{\tau}_h = (\rho D^3/8\gamma)^{1/2}$, that is, the transient conductive process characterized by $\boldsymbol{\tau}_e$ is not critical for the EWD actuation. This agrees with the experimental observation that the EWD-driven contact angle reduction is not sensitive to the liquid's electrolyte concentration thus the liquid conductivity [38].

During this transient conductive phase, the free floating charges within the droplets will accumulate at the droplet surface to support the aforementioned electric field discontinuity at the material boundaries. This surface charge density is directly linked with the applied voltage and the EWD force magnitude. Consequently, EWD is also referred to as a charge-controlled method.

The applicability of (7) is limited to a threshold value. Once the applied voltage exceeds this threshold value, the contact angle abruptly ceases from further decreasing. This contact angle saturation may be due to entrapped charges in the solid substrate which reduce the electric field intensity disparity along the contact line [39]. An alternative hypothesis is that

the electric resistivity of the liquid consumes the electric energy thus causing the contact angle saturation [40]. However, according to our analysis above, the electric current inside the droplet quickly reduces to zero once the electric equilibrium is established. The loss of the electrostatic energy stored in the dielectric coating due to the droplet's electric resistivity may not be able to sustain the contact angle saturation.

In addition to life science applications, EWD has also been applied to other areas such as display applications where the droplets are not necessarily aqueous, consequently, $\varepsilon_d \gg \varepsilon_a$ may not hold. In this case, the electrostatic energy stored inside the droplets cannot be safely discarded; both the conductivity and permittivity of the droplets need to be accounted for. A new set of the boundary conditions needs to be applied to the droplet surface instead of (6) [41]

$$\begin{aligned} &\boldsymbol{n} \cdot (\varepsilon_d \nabla \phi_a - \varepsilon_a \nabla \phi_a) = \sigma \\ &\frac{\partial \sigma}{\partial t} + \nabla_\Sigma \cdot \sigma \boldsymbol{v} + \boldsymbol{n} \cdot \kappa \nabla \phi_d = 0. \end{aligned} \tag{9}$$

Equation (7) provides a quick estimate for the EWD force discounting hydrodynamic effects. This type of order-of-magnitude analysis provides explicit descriptions of the impact of the design parameters on the first-order effects. Even though it may not be quantitatively accurate, it can be very useful to guide experimental design. A systematical study of this kind on EWD-based digital microfluidics has been reported by Song *et al.* [42]. For more rigorous solutions accounting for secondary effects, (4)–(6) need to be solved together with (1)–(3) simultaneously through numerical simulation means.

IV. Modeling and Simulation

A. Numerical Simulation Methods for Droplet Dynamics

The underlying mechanisms of most interfacial phenomena were qualitatively understood by 1970s. However, to this day quantitative analyses and descriptions of the many systems are still lacking. Modeling and numerical simulation approaches play a significant role in providing detailed quantification of the droplet dynamics. With the aid of the ever increasing computing power, numerical simulations are able to offer physical insights that are otherwise difficult to measure experimentally, provide evaluations of design performance and experimental strategies, and help to interpret experimental results.

One of the earliest works on numerical simulations of interfacial problems would be Birkhoff's work with Los Alamos Scientific Laboratory during 1950s. Prior to that, researchers relied on theoretical analysis based upon Rayleigh's interfacial stability theory (for instance, [43]). Even though, strictly speaking, this type of analysis is only applicable to small-disturbance linear problems; historically, the learning derived from this interfacial stability analysis was applied much more broadly, largely due to the unavailability of large-signal dynamics simulation tools and solutions until the computer was born.

The unique challenge in simulating droplet dynamics is to model the evolution of droplet surface and the topological change due to droplet breakup and/or droplet merge. There are two families of numerical schemes to describe the movement of the droplet surface. The Lagrangian approach distributes nodes on the droplet surface and tracks the droplet surface explicitly using interface-adaptive meshes. Examples of this approach include finite element method and boundary integral method. This Lagrangian approach provides sharp interface description; however, it faces insurmountable numerical challenge when the droplets undergo topological changes such as breakup and merge. The other approach, the Eulerian approach uses a function defined within a fixed numerical grid to describe the droplet surface. This approach captures the droplet surface by solving an additional transport equation therefore it is also referred to as front-capturing approach. Examples of this approach include marker-and-cell [44], volume-of-fluid [45], and level-set [46]. Because of the implicit nature of this family of interface-capturing schemes, complexities arise from interface reconstruction procedures. Volume-of-fluid may introduce undesired spurious currents if lower order interface reconstruction algorithm is used. Level-set method may fail to conserve mass in areas of high curvature. The advantage of the Eulerian approach is its capability of simulating topological changes of the droplet surface. A Lagrangian–Eulerian hybrid, the front-tracking method [47] was also developed. Its major drawback is the complexity of the associated interface reconstruction algorithms. The most recent addition to this collection of methods capable of simulating finite Reynolds number multiphase flows is the lattice Boltzmann method [48], of which, the accuracy and efficiency, comparing to more conventional methods, are still in active debate.

From the perspective of (pareto)-optimal balancing among accuracy, efficiency and practicality, the front-capturing methods are the favorite of the practitioners, in particular, volume-of-fluid, and level-set. In fact, almost all the leading commercial simulation packages that can be applied to digital microfluidics simulations implement some variations of these two methods. Examples include FLOW-3D (www.flow3d.com), CoventorWare (www.coventor.com), COMSOL (www.comsol.com), CFD-ACE+ (www.esi-group.com/products/Fluid-Dynamics/cfd-ace), and FLUENT (www.fluent.com). The simulation examples shown below were generated using CoventorWare (Coventor, Inc., Cambridge, MA) and FLOW-3D (Flow Science Inc., Santa Fe, NM) which implement volume-of-fluids methods.

The operation of many digital microfluidics platforms requires droplets being in direct contact with the surface of the solid substrate, also called the reaction surface. Different models of the droplet–surface interaction will provide different assessment of the viscous shear which affects the occurrence and the speed of the droplet movement hence the chip performance. The microfluidic nature of the droplet–surface interaction indicates a partial-slip boundary condition may be the most applicable. One example implementation may be as follows: two extreme cases are first implemented, that is, the no-slip condition for a very rough reaction surface that the liquid velocity at the reaction surface is set to zero, and the free-slip condition reflecting a perfect smooth surface that no tangential stresses are present at the reaction surface. An additional weight parameter is created to simulate surfaces in between the no-slip condition and free-slip condition.

This weight parameter is empirical and extracted from experimental measurements.

B. Example Simulations

As described above, modeling the topological change is one of the fundamental challenges for droplet dynamics simulations. Here we present such simulation example, that is, droplet fission process carried out by EWD-driven digital microfluidics [49].

As illustrated in Fig. 7, an individually addressable electrode array can be used to program desired electric field such that a spatial variation of the EWD force is generated at the tri-phase contact line. The net wetting force is then used to accomplish droplet generation, translocation, fission, and fusion. Fig. 7(a) shows the device configuration. The electrodes are aligned along the x-direction, and a droplet initially is centered in between two neighboring electrodes. Upon application of a voltage to all the electrodes, a spatial disparity of EWD force is created. Fig. 7(b) shows the simulation results. It can be observed that the contact angle at the tri-phase contact point closer to the electrodes (the vicinity of points W and E) is smaller than that at the tri-phase contact point further from the electrodes (the vicinity of points N and S). Consequently, the droplet is elongated in the x-direction at both sides (along W–E plane), and simultaneously the y–z cross-section at the center of the droplet (on N–S plane) is reduced. Eventually, the cross-section in the N–S plane reduces to a point and two droplets are created to conclude the fission process.

This section has been focused on detailed physical simulations of component-level operations. Such on-chip droplet operations are the key technology enablers; but in order to fulfill certain desired services, the components must be synthesized to form a functional system. System-level simulations are needed to address architectural and workflow level issues, such as job decomposition, job sequencing, job assignment, and component placement and routing (both electrically and fluidically) [50]. These system-level simulations use operational models, or behavioral models, to encapsulate the component-level complexities. Compared to the state of the art of CAD for microelectronics, the system-level modeling aid for microfluidics system design and integration is far less mature and presents a significant challenge and thus opportunity.

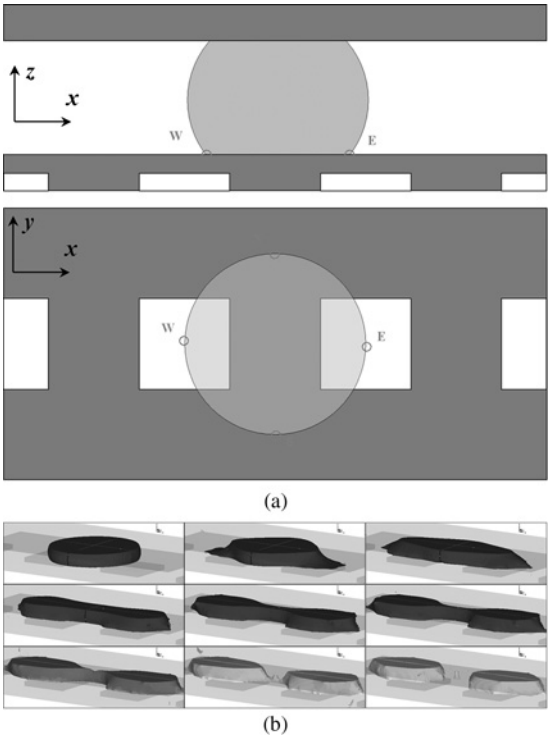

Fig. 7. Droplet fission on an EWD-driven lab-on-a-chip. (a) Device configuration. All four electrodes embedded in the insulating material are ON electrodes, 100 μm wide and 100 μm apart. The thickness of the insulating coating is 5 μm. (b) Simulation solution of the transient sequence of the droplet fission process. The snapshots are at a 75 μs time interval. Initially (without the presence of the electric field), this water-based droplet of 1 μL is of a "pancake" shape maintaining a contact angle of 117°. Upon application of 70-V to all four electrodes, the reduction of the contact angle elongates the droplet in the x-direction, shrinking the yz-plane cross-section at the center of the droplet, which eventually breaks the droplet into two parts (satellite droplets can also be observed) [49].

V. Synthesis Methods

In this section, we examine a progression of CAD problems related to biochip synthesis. A more detailed survey of CAD solutions is presented in [81].

A. Scheduling and Module Placement

Recent years have seen growing interest in the automated design and synthesis of microfluidic biochips [52], [56], [59]–[63], [65]–[68], [71]–[73], [74]–[78]. Optimization goals here include the minimization of assay completion time, minimization of chip area, and higher defect tolerance. The minimization of the assay completion time, i.e., the maximization of throughput, is essential for environmental monitoring applications where sensors can provide early warning. Real-time response is also necessary for surgery and neonatal clinical diagnostics. Finally, biological samples are sensitive to the environment and to temperature variations, and it is difficult to maintain an optimal clinical or laboratory environment on-chip. To ensure the integrity of assay results, it is therefore desirable to minimize the time that samples spend on-chip before assay results are obtained.

Increased throughput also improves operational reliability. Long assay durations imply that high actuation voltages need to be maintained on some electrodes, which accelerate insulator degradation and dielectric breakdown, reducing the number of assays that can be performed on a chip during its lifetime.

One of the first published methods for biochip synthesis decoupled high-level synthesis from physical design [56], [66]. Architectural-level synthesis for microfluidic biochips can be viewed as the problem of scheduling assay functions and binding them to a given number of resources so as to maximize parallelism, thereby decreasing response time. A behavioral model for a set of bioassays is first obtained from their laboratory protocols. Architectural-level synthesis is then used to generate a macroscopic structure of the biochip; this is analogous to a structural RTL model in electronic CAD [53]. On the other hand, geometry-level synthesis (physical design) addresses the placement of resources and the routing of droplets to satisfy objectives such as area or throughput. It

creates final layout of the biochip, consisting of the placement of microfluidic modules such as mixers and storage units, the routes that droplets take between different modules, and other geometrical details [65].

As in the case of high-level synthesis for ICs, resource binding in the biochip synthesis flow refers to the mapping from bioassay operations to available functional resources. Note that there may be several types of resources for any given bioassay operation. For example, a 2×2-array mixer, a 2×3-array mixer and a 2×4-array mixer can be used for a droplet mixing operation, but with different mixing times. In such cases, a resource selection procedure must be used. On the other hand, resource binding may associate one functional resource with several assay operations; this necessitates resource sharing. Once resource binding is carried out, the time duration for each bioassay operation can be easily determined. Scheduling determines the start times and stop times of all assay operations, subject to the precedence and resource-sharing constraints.

A key problem in the geometry-level synthesis of biochips is the placement of microfluidic modules such as different types of mixers and storage units. Since digital microfluidics-based biochips enable dynamic reconfiguration of the microfluidic array during run-time, they allow the placement of different modules on the same location during different time intervals. A simulated annealing-based heuristic approach has been developed to solve the NP-complete problem in a computationally efficient manner [65]. Solutions for the placement problem can provide the designer with guidelines on the size of the array to be manufactured. If module placement is carried out for a fabricated array, area minimization frees up more unit cells for sample collection and preparation.

Architectural synthesis is based on rough estimates for placement costs such as the area of the microfluidic modules. These estimates provide lower bounds on the exact biochip area, since the overheads due to spare cells and cells used for droplet transportation are not known a priori. However, it cannot be accurately predicted if the biochip design meets system specifications, e.g., maximum allowable array area and upper limits on assay completion times, until both high-level synthesis and physical design are carried out. [59] proposed a unified system-level synthesis method for microfluidic biochips based on parallel recombinative simulated annealing (PRSA), which offers a link between these two steps. This method allows users to describe bioassays at a high level of abstraction, and it automatically maps behavioral descriptions to the underlying microfluidic array.

The design flow is illustrated in Fig. 8. First, the different bioassay operations (e.g., mixing and dilution), and their mutual dependences are represented using a sequencing graph. Next, a combination of simulated annealing and genetic algorithms are used for unified resource binding, operation scheduling, and module placement. A chromosome is used to represent each candidate solution, i.e., a design point. In each chromosome, operations are randomly bound to resources. Based on the binding results, list scheduling is used to determine the start times of operations, i.e., each operation starts with a random latency after its scheduled time. Finally,

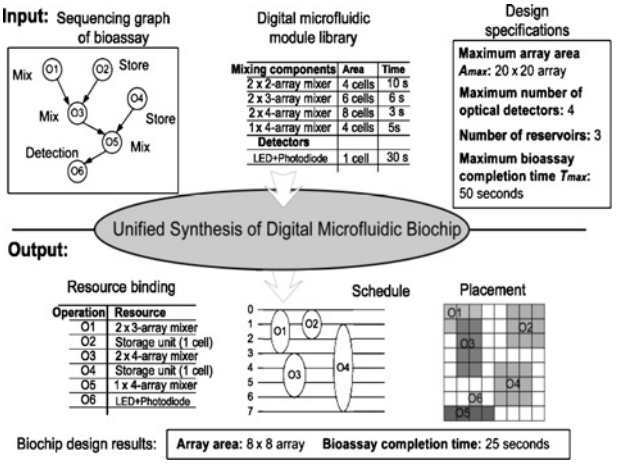

Fig. 8. Example illustrating system-level synthesis [59].

a module placement is derived based on the resource binding and the schedule of fluidic operations. A weighted sum of area and time-cost is used to evaluate the quality of the design. The design is improved through a series of genetic evolutions based on PRSA. It generates an optimized schedule of bioassay operations, the binding of assay operations to resources, and a layout of the microfluidic biochip.

Efficient reconfiguration techniques have been developed to bypass faulty unit cells in the microfluidic array [67]. A microfluidic module containing a faulty unit cell can easily be relocated to another part of the microfluidic array by changing the control voltages applied to the corresponding electrodes [61]. Defect tolerance can also be achieved by including redundant elements in the system; these elements can be used to replace faulty elements through reconfiguration techniques [60]. Another method is based on graceful degradation, in which all elements in the system are treated in a uniform manner, and no element is designated as a spare [62]. In the presence of defects, a subsystem with no faulty element is first determined from the faulty system. This subsystem provides the desired functionality, but with a gracefully degraded level of performance (e.g., longer execution times). Due to the dynamic reconfigurability of digital microfluidics-based biochips, microfluidic components (e.g., mixers) can be viewed as reconfigurable virtual devices. For example, a 2×4 array mixer (implemented using a rectangular array of control electrodes—two in the X-direction and four in the Y-direction) can easily be reconfigured to a 2×3 array mixer or a 2×2 array mixer.

The top-down synthesis flow described above unifies architecture level design with physical-level module placement. However, it suffers from two drawbacks. For operation scheduling, it is assumed that the time cost for droplet routing is negligible, which implies that droplet routing has no influence on the operation completion time. While generating physical layouts, the synthesis tool in [59] provides only the layouts of the modules and it leaves droplet routing pathways unspecified. The assumption of negligible droplet transportation times is valid for small microfluidic arrays. However, for large arrays and for biochemical protocols that require several

concurrent fluidic operations on-chip, the droplet transportation time is significant and routing complexity is non-trivial. This problem is addressed in the next section.

B. Droplet Routing

A key problem in biochip physical design is droplet routing between modules, and between modules and I/O ports (i.e., on-chip reservoirs). The dynamic reconfigurability inherent in digital microfluidics allows different droplet routes to share cells on the microfluidic array during different time intervals. In this sense, the routes in microfluidic biochips can be viewed as *virtual routes*, which make droplet routing different from the classical wire very large scale integration routing problem. Systematic routing method for digital microfluidic biochips have therefore been developed to minimize the number of cells used for droplet routing, while satisfying constraints imposed by performance goals and fluidic properties.

One of the first methods for droplet routing in biochips was published in [63]. The main objective in routing is to find droplet routes with minimum lengths, where route length is measured by the number of cells in the path from the starting point to the destination. For a microfluidic array of fixed size, minimum-length droplet routes lead to the minimization of the total number of cells used in droplet routing, thus freeing up more spare cells for fault tolerance. As in the case of electronic circuits, the fluidic ports on the boundary of microfluidic modules are referred to as *pins*. Similarly, we refer to the droplet routes between pins of different modules or on-chip reservoirs as *nets*. Thus, a fluidic route on which a single droplet is transported between two terminals can easily be modeled as a 2-pin net. We also need to move two droplets from different terminals to one common microfluidic module (e.g., mixer) for mixing. To allow droplet mixing simultaneously during their transport, we need to model such fluidic routes using 3-pin nets.

During droplet routing, a minimum spacing between droplets must be maintained to prevent accidental mixing, except for the case when droplet merging is desired (e.g., in 3-pin nets). Fluidic constraint rules in [63] need to be satisfied in order to avoid undesirable mixing. We view the microfluidic modules placed on the array as *obstacles* in droplet routing. In order to avoid conflicts between droplet routes and assay operations, a segregation region is added to wrap around the functional region of microfluidic modules. Another constraint in droplet routing is given by an upper limit on droplet transportation time. The delay for each droplet route should not exceed some maximum, e.g., 10% of a time-slot used in scheduling, in order that the droplet-routing time can be ignored for scheduling assay operations [63].

Since a digital microfluidic array can be reconfigured dynamically at run-time, a series of 2-D placement configurations of modules in different time spans are obtained in the module placement phase [60]. Therefore, the droplet routing is decomposed into a series of sub-problems. We obtain a complete droplet-routing solution by solving these sub-problems sequentially.

Based on this problem formulation, a two-stage routing method has been proposed in [63]. In the first stage, M alternative routes for each net are generated. In the second stage, a single route from the M alternatives for each net is selected independent of the routing order of nets. This method also exploits the features of dynamic reconfigurability and independent controllability of electrodes to modify droplet pathways to override potential violation of fluidic constraints.

Droplet routing should be considered in the synthesis flow for digital microfluidics, in order to generate a routable synthesized design for the availability of routing paths. [71] proposed a method to incorporate droplet-routability in the PRSA-based synthesis flow. This method estimates the droplet-routability using two metrics. It adopts the average module distance (over all interdependent modules) as the first design metric to guarantee the routability of modules in the synthesized biochip. It also adopts the maximum module distance as the second design metric to approximate the maximum length of droplet manipulation. Since synthesis results with high routability values are more likely to lead to simple and efficient droplet pathways, this method incorporates the above two metrics into the fitness function by a factor that can be fine-tuned according to different design specifications to control the PRSA-based procedure. For each chromosome considered in the PRSA-based synthesis flow, this method calculates both the average and maximum module distance. Candidate designs with low routability are discarded during evolution. Thus, the synthesis procedure guarantees that the routing complexity is reduced for the synthesized biochip, while meeting constraints on array size and bioassay processing time.

We ran the defect-tolerant routing-aware and defect-oblivious routing-aware algorithms under a set of combinations of weights in the fitness function for the protein assay example. We carried out random defect injection into each design and obtain its failure rate. We mapped each design G to a 3-D point (T_G, A_G, F_G), where T_G, A_G, F_G are completion time, chip area, and failure rate of the design, respectively. A point (T_G, A_G, F_G) is referred to as a feasibility boundary point if there are no other points (T_m, A_m, F_m) such that $T_m < T_G$, $A_m < A_G$, and $F_m < F_G$. A feasibility frontier surface is obtained by connecting all the feasibility boundary points, as shown in Fig. 9. The feasible design region corresponds to the space above the feasible surface. Any design specification can be met whose corresponding is point located in this region; otherwise, no feasible design exists for this specification. As shown in Fig. 9, defect-tolerant routing-aware synthesis leads to a lower-feasibility frontier surface and a larger feasible design space as compared to the defect-oblivious method.

VI. Pin-Constrained Chip Design

Electrode addressing is an important problem in biochip design. It refers to the manner in which electrodes are connected to and controlled by input pins. Early design-automation techniques relied on the availability of a direct-addressing scheme. For large arrays, direct-addressing schemes lead to a large number of control pins, and the associated interconnect

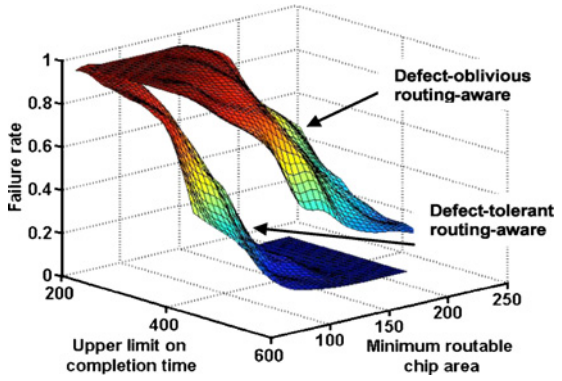

Fig. 9. Feasibility frontier surface and feasible design region for defect-tolerant and defect-oblivious routing-aware synthesis methods [73].

routing problem significantly adds to the product cost. Thus, the design of pin-constrained digital microfluidic arrays is of great practical importance for the emerging marketplace. In this section, we describe a number of pin-constrained biochip design methods.

A. Droplet-Trace-Based Array Partitioning

An array-partitioning-based pin-constrained design method of digital microfluidic biochips proposed in [68]. This method uses array partitioning and careful pin assignment to reduce the number of control pins. The key idea is to "virtually" partition the array into regions. The partitioning criterion here is to ensure at most one droplet is included in each partition. The droplet trace, defined as the set of cells traversed by a single droplet, serves as the basis for generating the array partitions. The droplet trace can be easily extracted from the droplet routing information and the placement of the modules to which it is routed. If droplets traces intersect on the array, the partitions derived by this method overlap in some regions. Sets of pins from an "overlapping" partition cannot be used in the overlapped region since the reuse of the pins may lead to droplet interference. The solution to this problem is to make the overlapping region a new partition, referred to as the overlapping partition, and use direct addressing (one-to-one mapping) for it.

A Connect-5 algorithm is used to address the problem of how to map control pins to the electrodes in a partition, which can be easily implemented using a 3-layer-PCB. The Connect-5 algorithm succeeds in avoiding droplet interference while moving a single droplet inside the partition. It can be integrated into the droplet-trace-based array partitioning method to generate droplet-interference-free layouts with a minimum number of pins. However, this method requires detailed information about the scheduling of assay operations, microfluidic module placement, and droplet routing pathways. Thus, the array design in such cases is specific to a target biofluidic application.

B. Cross-Referencing-Based Droplet Manipulation

An alternative method based on a cross-reference driving scheme is presented in [72]. This method allows control of an $N \times M$ grid array with only $N+M$ control pins. The electrode rows are patterned on both the top and bottom plates, and placed orthogonally. In order to drive a droplet along the X-direction, electrode rows on the bottom plate serve as driving electrodes, while electrode rows on the top serve as reference ground electrodes. The roles are reversed for movement along the Y-direction. This cross-reference method facilitates the reduction of control pins. However, due to electrode interference, this design cannot handle the simultaneous movement of more than two droplets. For the concurrent manipulation of multiple droplets on a cross-referencing-based biochip, multiple row and column pins must be selected to activate the destination cells, i.e., cells to which the droplets are supposed to move. However, the selected row and column pins may also result in the activation of cells other than the intended droplet destinations.

A solution based on destination-cell categorization is proposed to tackle the above problem. The key idea is to group the droplet movements according to their destination cells. A group consists of droplets whose destination cells share the same column or row. In this way, the manipulation of multiple droplets is ordered in time; droplets in the same group can be moved simultaneously without electrode interference, but the movements for the different groups must be sequential. The problem of finding the minimum number of groups can be directly mapped to the problem of determining a minimal clique partition from graph theory [51]. A linear-time heuristic algorithm based on row-scanning and column-scanning has been used to derive the clique partitions.

C. Broadcast-Addressing Method

One drawback of the cross-reference driving scheme is that this design requires a special electrode structure (i.e., both top and bottom plates contain electrode rows), which results in increased manufacturing cost. Thereby, a broadcast-addressing based design technique for pin-constrained and multi-functional biochips has been developed in [73].

To execute a specific bioassay, routing and scheduling information must be stored in the form of electrode activation sequences, where each bit representing the status of the electrode at a specific time-step. The status can be either "1" (activate), "0" (deactivate) or "F" (floating). The "floating" status is represented using the symbol "x" and refer to it as "don't-care." Each electrode activation sequence contains several don't-care terms, which can be replaced by "1" or "0." If two sequences can be made identical by careful replacing these don't-care terms with "0" or "1," they are referred to as *compatible sequences*. Compatible sequences can be generated from a single signal source.

The number of control pins can be reduced by connecting together electrodes with mutually compatible activation sequences, and addressing them using a single control pin. Therefore, the resulting electrode-access method is referred to as a *broadcast addressing*. The first step here is to partition the electrodes into groups. For all the electrodes in any group, the corresponding activation sequences must be pairwise-compatible. The problem of finding an optimal partition that leads to the minimum number of groups can be easily mapped to the problem of determining a minimal clique partition from

TABLE I
EXAMPLES OF FAULT MODELS FOR DIGITAL MICROFLUIDIC BIOCHIP [71]

Cause of Defect	Defect Type	Number of Cells	Fault Model	Observable Error
Excessive actuation voltage applied to an electrode	Dielectric breakdown	1	Droplet–electrode short (a short between the droplet and the electrode)	Droplet undergoes electrolysis, which prevents its further transportation
Electrode actuation for excessive duration	Irreversible charge concentration on an electrode	1	Electrode-stuck-on (the electrode remains constantly activated)	Unintentional droplet operations or stuck droplets
Excessive mechanical force applied to the chip	Misalignment of parallel plates (electrodes and ground plane)	1	Pressure gradient (net static pressure in some direction)	Droplet transportation without activation voltage
Coating failure	Non-uniform dielectric layer	1	Dielectric islands (islands of Teflon coating)	Fragmentation of droplets and their motion is prevented
Abnormal metal layer deposition and etch variation during fabrication	Grounding Failure	1	Floating droplets (droplet are not anchored)	Failure of droplet transportation
	Broken wire to control source	1	Electrode open (electrode actuation is not possible)	Failure to activate the electrode for droplet transportation
	Metal connection between two adjacent electrodes	2	Electrode short (short between electrodes)	A droplet resides in the middle of the two shorted electrodes, and its transport along one or more directions cannot be achieved
Particle contamination or liquid residue	A particle that connect two adjacent electrodes	2	Electrode short	
Protein adsorption during bioassay [10]	Sample residue on electrode surface	1	Resistive open at electrode	Droplet transportation is impeded
			Contamination	Assay results are outside the range of possible outcomes

graph theory [51]. The minimum number of groups yields the minimum number of control pins.

VII. TESTING

In this section, we describe recent advances in the testing of digital microfluidic biochips and fault localization techniques. Test techniques for ICs cannot be directly applied to microfluidic biochips, since they do not handle fluids. Due to their underlying mixed technology and multiple energy domains, microelectrofluidic systems exhibit failure mechanisms and defects that are significantly different from the failure modes in analog ICs.

A. Fault Modeling

As in microelectronic circuits, a defective microfluidic biochip is said to have a failure if its operation does not match its specified behavior [54]. In order to facilitate the detection of defects, fault models that efficiently represent the effect of physical defects at some level of abstraction are required. These models can be used to capture the effect of physical defects that produce incorrect behaviors in the electrical or fluidic domain. As described in [55], faults in digital microfluidic systems can be classified as being either catastrophic or parametric. Catastrophic faults lead to a complete malfunction of the system, while parametric faults cause degradation in the system performance. A parametric fault is detectable only if this deviation exceeds the tolerance in system performance.

Catastrophic faults may be caused by a number of physical defects, and examples are as follows.

1) *Dielectric breakdown:* The breakdown of the dielectric at high voltage levels creates a short between the droplet and the electrode. When this happens, the droplet undergoes electrolysis, thereby preventing further transportation.
2) *Short between the adjacent electrodes:* If a short occurs between two adjacent electrodes, the two electrodes effectively form one longer electrode. When a droplet resides on this electrode, it is no longer large enough to overlap the gap between adjacent electrodes. As a result, the actuation of the droplet can no longer be achieved.
3) *Degradation of the insulator:* This degradation effect is unpredictable and may become apparent gradually during the operation of the microfluidic system. A consequence is that droplets often fragment and their motion is prevented because of the unwanted variation of surface tension forces along their flow path.
4) *Open in the metal connection between the electrode and the control source:* This defect results in a failure in activating the electrode for transport.

Table I lists some common failure sources, defects, and the corresponding fault models for catastrophic faults in digital microfluidic lab-on-chip. Examples of some common parametric faults include the following.

1) *Geometrical parameter deviation:* The deviation in insulator thickness, electrode length and height between parallel plates may exceed their tolerance value.
2) *Change in viscosity of droplet and filler medium:* These can occur during operation due to an unexpected biochemical reaction, or changes in operational environment, e.g., temperature variation.

B. Structural Test Techniques

A unified test methodology for digital microfluidic biochips has recently been presented, whereby faults can be detected by controlling and tracking droplet motion electrically [57]. Test stimuli droplets containing a conductive fluid (e.g., KCL solution) are dispensed from the droplet source. These droplets are guided through the unit cells following the test plan toward the droplet sink, which is connected to an integrated capacitive detection circuit. Most catastrophic faults result in a complete cessation of droplet transportation. Therefore, we can determine the fault-free or faulty status of the system by simply observing the arrival of test stimuli droplets at selected ports. An efficient test plan ensures that testing does not conflict with the normal bioassay, and it guides test stimuli droplets to cover all the unit cells available for testing. The microfluidic array can be modeled as an undirected graph, and the pathway for the test droplet can be determined by solving the Hamiltonian path problem [64]. With negligible hardware overhead, this method also offers an opportunity to implement self-test for microfluidic systems and therefore eliminate the need for costly, bulky, and expensive external test equipment. Furthermore, after detection, droplet flow paths for bioassays can be reconfigured dynamically such that faulty unit cells are bypassed without interrupting the normal operation.

Even though most catastrophic faults lead to a complete cessation of droplet transportation, there exist differences between their corresponding erroneous behaviors. For instance, to test for the electrode-open fault, it is sufficient to move a test droplet from any adjacent cell to the faulty cell. The droplet will always be stuck during its motion due to the failure in charging the control electrode. On the other hand, if we move a test droplet across the faulty cells affected by an electrode-short fault, the test droplet may or may not be stuck depending on its flow direction. Therefore, to detect such faults, it is not enough to solve only the Hamiltonian path problem. In [58], a solution based on Euler paths in graphs is described for detecting electrode shorts.

Despite its effectiveness for detecting electrode shorts, testing based on an Euler path suffers from long test application time. This approach uses only one droplet to traverse the microfluidic array, irrespectively of the array size. Fault diagnosis is carried out by using multiple test application steps and adaptive Euler paths. Such a diagnosis method is inefficient since defect-free cells are tested multiple times. Moreover, the test method leads to a test plan that is specific to a target biochip. If the array dimensions are changed, the test plan must be completely altered. In addition, to facilitate chip testing in the field, test plans need to be programmed into a microcontroller. However, the hardware implementations of test plans from [57] are expensive, especially for low cost, disposable biochips. More recently, a cost-effective testing methodology referred to as "parallel scan-like test" has been proposed [70]. The method is named thus because it manipulates multiple test droplets in parallel to traverse the target microfluidic array, just as test stimuli can be applied in parallel to the different scan chains in an IC.

The parallel scan-like test method has been applied to a fabricated biochip. The chip-under-test is a PCB microfluidic platform for DNA sequencing, as shown in Fig. 10. The platform consists of a 7×7 array, eight reservoirs and routing electrodes that connect reservoirs to the array. A total of nine cells are reserved for grounding, and they are not available for droplet transportation. As a baseline, Euler-path-based testing was applied to this chip [70]. The test procedure takes 57 s, assuming a (typical) 1 Hz electrode-actuation frequency. Next, parallel scan-like test was applied to this chip. The test application procedure takes 46 s, again for a 1 Hz actuation frequency.

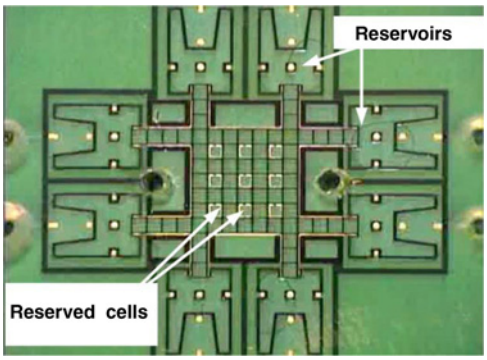

Fig. 10. Fabricated lab-on-chip for DNA sequencing used to demonstrate parallel scan-like testing [70].

Next, we evaluate the time needed for fault diagnosis for the two methods. In [70], a fabricated chip was used, which was known a priori to contain one defect. For the Euler-path-based method, binary search was carried out to locate the defective cell. A total of seven iterations were needed and the total diagnosis time was 173 s. On the other hand, parallel scan-like test can simply determine the defect site from test-outcome readouts. No additional diagnosis steps are needed and the diagnosis time is the same as the testing time, i.e., 44 s, which correspond to a 75% reduction compared to [57].

A drawback of the above "structural" test methods is that they focus only on physical defects, and they overlook module functionality. Therefore, these methods can only guarantee that a biochip is defect-free. However, a defect-free microfluidic array can also malfunction in many ways. For example, a defect-free reservoir may result in large volume variations when droplets are dispensed from it. A splitter composed of three defect-free electrodes may split a big droplet into two droplets with significantly unbalanced volumes. These phenomena, referred to as malfunctions, are not the result of electrode defects. Instead, they are activated only for certain patterns of droplet movement or fluidic operations. Such malfunctions can have serious consequences on the integrity of bioassay results.

C. Functional Testing Techniques

Functional testing involves test procedures to check whether groups of cells can be used to perform certain operations, e.g., droplet mixing and splitting. For the test of a specific operation, the corresponding patterns of droplet movement are carried out on the target cluster of cells. If a target cell cluster fails the test, e.g., the mixing test, we label it as a malfunctioning cluster. As in the case of structural testing, fault models must be developed for functional testing.

TABLE II
FUNCTIONAL FAULT MODELS [57]

Cause of Malfunction	Malfunction Type	Numberof Cells	Fault Model	Observable Error
Electrode actuation for excessive duration	Irreversible charge concentration on the dispensing electrode	3	Dispensing-stuck-on (droplet is dispensed by not fully cut off from the reservoir)	No droplet can be dispensed from the reservoir
Electrode shape variation in fabrication	Deformity of electrodes	3	No overlap between droplets to be mixed and center electrode	Mixing failure
Electrode electrostatic property variation in fabrication	Unequal actuation voltages	3	Pressure gradient (net static pressure in some direction)	Unbalanced volumes of split droplets
Bad soldering	Parasitic capacitance in the capacitive sensing circuit	1	Oversensitive or insensitive capacitive sensing	False positive/negative in detection

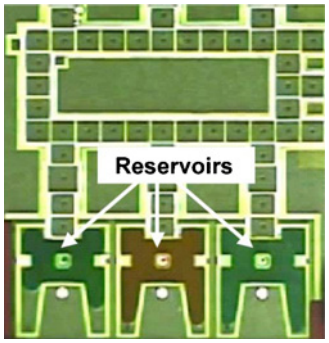

Fig. 11. Fabricated lab-on-chip used for PCR [57].

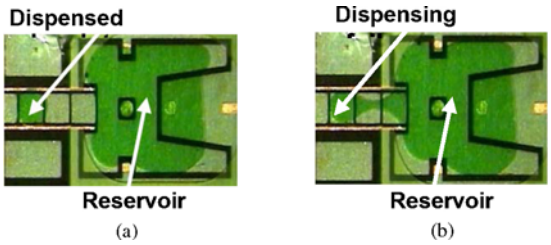

Fig. 12. Illustration of (a) normal dispensing and (b) dispensing failure, for a fabricated lab-on-chip [57].

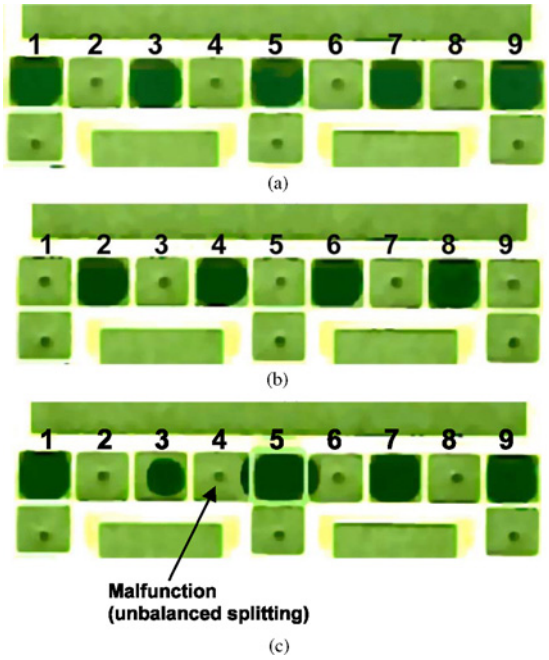

Fig. 13. (a)–(c) Mixing and splitting test for a fabricated PCR chip [57].

Malfunctions in fluidic operations are identified and included in the list of faults; see Table II.

Functional test methods to detect the defects and malfunctions have recently been developed. In particular, dispensing test, mixing test, splitting test, and capacitive sensing test have been described in [69] to address the corresponding malfunctions.

Functional test methods were applied to a PCB microfluidic platform for the PCR, as shown in Fig. 11. The platform consists of two columns and two rows of electrodes, three reservoirs, and routing electrodes that connect the reservoirs to the array. A dispensing malfunction is shown in Fig. 12.

An illustration of the mixing and splitting test is shown in Fig. 13. The bottom row was first targeted and five test droplets were dispensed to the odd electrodes, as shown in Fig. 13(a). Next, splitting test for the even electrodes was carried out. Droplets were split and merged on the even electrodes. In Fig. 13(b), we see a series of droplets of the same volume resting on the even electrodes, which means that all the odd electrodes passed the splitting test, and merging at the even electrodes worked well. However, when the splitting test was carried out on the even electrodes, a large variation in droplet volume was observed on the third and fifth electrodes (see Fig. 13(c)). This variation implied a malfunction, leading to unbalanced splitting on the 4th electrode. The malfunction was detected when the droplets were routed to the capacitive sensing circuit. The fourth electrode on the bottom row was marked as an unqualified splitting site.

VIII. CONCLUSION

We have presented a survey of research on design tools for digital microfluidic biochips. We first provided an overview of the digital microfluidic platform, and highlighted emerging applications. Advances in modeling, simulation, synthesis and droplet routing techniques have been described. Practical design techniques for achieving high throughout with a small number of control pins have been presented. Testing and design-for-testability techniques have also been presented. Common defects have been identified and related to logical

fault models. Based on these fault models, test techniques for emerging biochip devices and digital microfluidic modules have been presented. The use of these test techniques for fabricated devices has been highlighted. These design techniques are expected to pave the way for the deployment and use of biochips in the emerging marketplace. There is a need for continued design automation and testing research for emerging biochips. CAD research is especially relevant in the context of cross-contamination between samples, synthesis and optimization under pin-count constraints, in-system error detection and automated error recovery, and control-flow leading to decision-tree architectures.

The CAD community now has access to assay "benchmarks" for biochips CAD research [80] and these are currently being used by research groups in the U.S., Taiwan, and Denmark. Biochips CAD software is also available for distribution upon request. Experimental research and validation requires extensive laboratory setup, but prototype chips and experimental facilities are available at Advanced Liquid Logic and at Duke University, Durham, NC.

REFERENCES

[1] T. H. Schulte, R. L. Bardell, and B. H. Weigl, "Microfluidic technologies in clinical diagnostics," *Clin. Chim. Acta*, vol. 321, no. 1, pp. 1–10, 2002.

[2] V. Srinvasan, V. K. Pamula, M. G. Pollack, and R. B. Fair, "Clinical diagnostics on human whole blood, plasma, serum, urine, saliva, sweat, and tears on a digital microfluidic platform," in *Proc. MicroTAS*, 2003, pp. 1287–1290.

[3] A. Guiseppi-Elie, S. Brahim, G. Slaughter, and K. R. Ward, "Design of a subcutaneous implantable biochip for monitoring of glucose and lactate," *IEEE Sensors J.*, vol. 5, no. 3, pp. 345–355, Jun. 2005.

[4] R. B. Fair, A. Khlystov, T. D. Tailor, V. Ivanov, R. D. Evans, P. B. Griffin, V. Srinivasan, V. K. Pamula, M. G. Pollack, and J. Zhou, "Chemical and biological applications of digital-microfluidic devices," *IEEE Design Test Comput.*, vol. 24, no. 1, pp. 10–24, Jan.–Feb. 2007.

[5] E. A. Ottesen, J. W. Hong, S. R. Quake, and J. R. Leadbetter, "Microfluidic digital PCR enables multigene analysis of individual environmental bacteria," *Science*, vol. 314, no. 5804, pp. 1464–1467, 2006.

[6] Y. Zhao and S. K. Cho, "Microparticle sampling by electrowetting actuated droplet sweeping," *Lab Chip*, vol. 6, no. 1, pp. 137–144, 2006.

[7] V. Srinivasan, V. K. Pamula, and R. B. Fair, "An integrated digital microfluidic lab-on-a-chip for clinical diagnostics on human physiological fluids," *Lab Chip*, vol. 4, no. 4, pp. 310–315, 2004.

[8] E. Verpoorte and N. F. D. Rooij, "Microfluidics meets MEMS," *Proc. IEEE*, vol. 91, no. 6, pp. 930–953, Jun. 2003.

[9] *International Technology Roadmap for Semiconductors (ITRS)*. Semiconductor Industry Association, San Jose, CA, 2007 [Online]. Available: http://www.itrs.net/Links/2007ITRS/Home2007.htm

[10] M. G. Pollack, R. B. Fair, and A. D. Shenderov, "Electrowetting-based actuation of liquid droplets for microfluidic applications," *Appl. Phys. Lett.*, vol. 77, no. 11, pp. 1725–1727, 2000.

[11] J. Lee, H. Moon J. Fowler, C.-J. Kim, and T. Schoellhammer, "Addressable micro liquid handling by electric control of surface tension," in *Proc. Int. Conf. MEMS*, 2001, pp. 499–502.

[12] S.-K. Cho, S.-K. Fan, H. Moon, and C.-J. Kim, "Toward digital microfluidic circuits: Creating, transporting, cutting and merging liquid droplets by electrowetting-based actuation," in *Proc. TechDig MEMS Intl. Conf.*, 2002, pp. 11454–11461.

[13] P. R. C. Gascoyne and J. V. Vykoukal, "Dielectrophoresis based sample handling in general-purpose programmable diagnostic instruments," *Proc. IEEE*, vol. 92, no. 1, pp. 22–42, Jan. 2004.

[14] D. A. Anton, J. P. Valentino, S. M. Trojan, and S. Wagner, "Thermocapillary actuation of droplets on chemically patterned surfaces by programmable microheater arrays," *J. Microelectromech. Syst.*, vol. 12, no. 6, pp. 873–879, 2003.

[15] A. Renaudin, P. Tabourier, V. Zhang, C. Druhon, and J. C. Camart, "Plateforme SAW dédiée à la microfluidique discrète pour applications biologiques," in *Proc. Congrès Français de Microfluidique, Société Hydrotechnique de France*, 2004, pp. 14–16.

[16] A. Manz, N. Graber, and H. M. Widmer, "Miniaturized total chemical analysis systems: A novel concept for chemical sensing," *Sens. Act. B*, vol. 1, nos. 1–6, pp. 244–248, 1990.

[17] J. Ding, K. Chakrabarty, and R. B. Fair, "Scheduling of microfluidic operations for reconfigurable 2-D electrowetting arrays," *IEEE Trans. Comput.-Aided Design Integr. Circuits Syst.*, vol. 29, no. 12, pp. 1463–1468, Dec. 2001.

[18] B. Berge, "Electrocapillarite et mouillage de films isolants par l'eau," *C. R. Acad. Sci. II*, vol. 317, no. 2, pp. 157–163, 1993.

[19] F. Su, K. Chakrabarty, and R. B. Fair, "Microfluidics-based biochips: Technology issues, implementation platforms, and design automation challenges," *IEEE Trans. Comput.-Aided Design Integr. Circuits Syst.*, vol. 25, no. 2, pp. 211–223, Feb. 2006.

[20] V. Srinivasan, V. K. Pamula, and R. B. Fair, "An integrated digital microfluidic lab-on-a-chip for clinical diagnostics on human physiological fluids," *Lab Chip*, vol. 4, no. 4, pp. 310–315, 2004.

[21] J. Aizenberg, T. Krupenkin, and P. Kolodner, "Accelerated chemical reactions for lab-on-a-chip applications using electrowetting-induced droplet self oscillations," in *Proc. Mater. Res. Soc. Symp.*, vol. 915. 2006, pp. 103–111.

[22] M. J. Madou and R. Cubicciotti, "Scaling issues in chemical and biological sensors," *Proc. IEEE*, vol. 91, no. 6, pp. 830–838, Jun. 2003.

[23] P. Thwar, J. L. Rouse, A. E. Eckhardt, P. Griffin, M. G. Pollack, and R. B. Fair, "Digital microfluidic DNA sequencing," in *Proc. AGBT Meeting*, Marco Island, FL, Feb. 2009.

[24] L. Luan, R. D. Evans, D. Schwinn, R. B. Fair, and N. M. Jokerst, "Chip scale integration of optical microresonator sensors with digital microfluidics systems," in *Proc. IEEE LEOS*, Nov. 9–13, 2008, pp. 259–260.

[25] S. Dhar, S. Drezdzon, and E. Maftei, "Digital microfluidic biochip for malaria detection," 2008, unpublished.

[26] G. Hu and D. Li, "Multiscale phenomena in microfluidics and nanofluidics," *Chemical Engineering Science*, vol. 62, no. 13, pp. 3443–3454, 2007.

[27] L. G. Leal, *Laminar Flow and Convective Transport Processes: Scaling Principles and Asymptotic Analysis*. Boston, MA: Butterworth-Heinemann, 1992.

[28] A. W. Adamson and A. P. Gast, *Physical Chemistry of Surfaces*. New York: Wiley, 1997.

[29] A. A. Darhuber, J. P. Valention, S. M. Troian, and S. Wagner, "Thermocapillary actuation of droplets on chemically patterned surfaces by programmable microheater arrays," *J. Microelectromech. Syst.*, vol. 12, no. 6, pp. 873–879, 2003.

[30] K. T. Katz, K. A. Noble, and G. W. Faris, "Optical microfluidics," *Appl. Phys. Lett.*, vol. 85, no. 13, pp. 2658–2660, 2004.

[31] P. Garstecki, M. J. Fuerstman, H. A. Stone, and G. M. Whitesides, "Formation of droplets and bubbles in a microfluidic T-junction: Scaling and mechanism of breakup," *Lab Chip*, vol. 6, no. 3, pp. 437–446, 2006.

[32] U. Lehmann, S. Hadjidj, V. K. Parashar, C. Vandevyver, A. Rida, and M. A. M. Gijs, "2-D magnetic manipulation of microdroplets on a chip as a platform for bioanalytical applications," *Sensors and Actuators B: Chemical*, vol. 117, no. 2, pp. 457–463, 2006.

[33] J. A. Schwartz, J. V. Vykoukal, and P. R. C. Gascoyne, "Droplet-based chemistry on a programmable micro-chip," *Lab Chip*, vol. 4, no. 1, pp. 11–17, 2004.

[34] R. Sista, Z. Hua, P. Thwar, A. Sudarsan, V. Srinivasan, A. Eckhardt, M. Pollack, and V. Pamula, "Development of a digital microfluidic platform for point of care testing," *Lab Chip*, vol. 8, no. 12, pp. 2091–2104, 2008.

[35] J. Zeng and F. T. Korsmeyer, "Principles of droplet electrohydrodynamics for lab-on-a-chip," *Lab Chip*, vol. 4, no. 4, pp. 265–277, 2004

[36] H. A. Haus and J. R. Melcher, *Electromagnetic Fields and Energy*. Englewood Cliffs, NJ: Prentice-Hall, 1989.

[37] R. B. Fair, "Digital microfluidics: Is a true lab-on-a-chip possible?" *Microfluidics and Nanofluidics*, vol. 3, no. 3, pp. 245–281, 2007.

[38] V. Peykov, A. Quinn, and J. Ralston, "Electrowetting: A model for contact-angle saturation," *Colloid and Polymer Science*, vol. 278, no. 8, pp. 789–793, 2000.

[39] H. J. J. Verheijen and M. W. J. Prins, "Reversible electrowetting and trapping of charge: Model and experiments," *Langmuir*, vol. 15, no. 20, pp. 6616–6620, 1999.

[40] B. Shapiro, H. Moon, R. L. Garrell, and C.-J. Kim, "Equilibrium behavior of sessile drops under surface tension, applied external fields, and material variations," *J. Appl. Phys.*, vol. 93, no. 9, pp. 5794–5811, 2003.

[41] J. R. Melcher and G. I. Taylor, "Electrohydrodynamics: A review of the role of interfacial shear stresses," *Annu. Rev. Fluid Mech.*, vol. 1, no. 1, pp. 111–146, 1969.
[42] J. H. Song, R. Evans, Y.-Y. Lin, B.-N. Hsu, and R. B. Fair, "A scaling model for electrowetting-on-dielectric microfluidic actuators," *Microfluidics Nanofluidics*, vol. 7, no. 1, pp. 75–89, 2009.
[43] J. B. Keller, S. I. Rubinow, and Y. O. Tu, "Spatial instability of a jet," *Phys. Fluids*, vol. 16, no. 12, pp. 2052–2055, 1973.
[44] F. H. Harlow and J. E. Welch, "Numerical study of large amplitude free surface motions," *Phys. Fluids*, vol. 9, no. 5, pp. 842–851, 1966.
[45] C. W. Hirt and B. D. Nichols, "Volume of fluid (VOF) method for the dynamics of free boundaries," *J. Comput. Phys.*, vol. 39, no. 1, pp. 201–225, 1981.
[46] J. A. Sethian, *Level Set Methods and Fast Marching Methods: Evolving Interfaces in Computational Geometry, Fluid Mechanics, Computer Vision, and Materials Science*. Cambridge, U.K.: Cambridge Univ. Press, 1999.
[47] S. O. Unverdi and G. Tryggvason, "A front-tracking method for viscous, incompressible, multi-fluid flows," *J. Comput. Phys.*, vol. 100, no. 1, pp. 25–37, 1992.
[48] X. W. Shan and H. D. Chen, "Lattice Boltzmann model for simulation flows with multiple phases and components," *Phys. Rev. E*, vol. 47, no. 3, pp. 1815–1819, 1993.
[49] J. Zeng, "Modeling and simulation of electrified droplets and its application to computer-aided design of digital microfluidics," *IEEE Trans. Comput.-Aided Design Integr. Circuits Syst.*, vol. 25, no. 2, pp. 224–233, Feb. 2006.
[50] K. Chakrabarty and F. Su, *Digital Microfluidic Biochips: Synthesis, Testing, and Reconfiguration Techniques*. Boca Raton, FL: CRC Press, 2006.
[51] R. Diestel, *Graph Theory*. Berlin, Germany: Springer, 2005.
[52] E. Maftei, P. Pop, J. Madsen, and T. Stidsen, "Placement-aware architectural synthesis of digital microfluidic biochips using ILP," in *Proc. Int. Conf. Very Large Scale Integr. Syst. Chip*, 2008, pp. 425–430.
[53] G. De Micheli, *Synthesis and Optimization of Digital Circuits*. New York: McGraw-Hill, 1994.
[54] H. G. Kerkhoff, "Testing of microelectronic-biofluidic systems," *IEEE Design Test Comput.*, vol. 24, no. 1, pp. 72–82, Jan.–Feb. 2007.
[55] F. Su, S. Ozev, and K. Chakrabarty, "Testing of droplet-based microelectrofluidic systems," in *Proc. IEEE Int. Test Conf.*, 2003, pp. 1192–1200.
[56] F. Su and K. Chakrabarty, "Architectural-level synthesis of digital microfluidics-based biochips," in *Proc. IEEE Int. Conf. CAD*, 2004, pp. 223–228.
[57] F. Su, S. Ozev, and K. Chakrabarty, "Ensuring the operational health of droplet-based microelectrofluidic biosensor systems," *IEEE Sens.*, vol. 5, no. 4, pp. 763–773, Aug. 2005.
[58] F. Su, W. Hwang, A. Mukherjee, and K. Chakrabarty, "Testing and diagnosis of realistic defects in digital microfluidic biochips," *J. Electron. Test.: Theory Appl.*, vol. 23, pp. 219–233, Jun. 2007.
[59] F. Su and K. Chakrabarty, "Unified high-level synthesis and module placement for defect-tolerant microfluidic biochips," in *Proc. IEEE/ACM Design Automat. Conf.*, 2005, pp. 825–830.
[60] F. Su and K. Chakrabarty, "Design of fault-tolerant and dynamically-reconfigurable microfluidic biochips," in *Proc. DATE Conf.*, 2005, pp. 1202–1207.
[61] F. Su and K. Chakrabarty, "Reconfiguration techniques for digital microfluidic biochips," in *Proc. Design, Test, Integr. Packag. MEMS/MOEMS Symp.*, 2005, pp. 143–148.
[62] F. Su and K. Chakrabarty, "Defect tolerance for gracefully-degradable microfluidics-based biochips," in *Proc. IEEE VLSI Test Symp.*, 2005, pp. 321–326.
[63] F. Su, W. Hwang, and K. Chakrabarty, "Droplet routing in the synthesis of digital microfluidic biochips," in *Proc. DATE Conf.*, 2006, pp. 323–328.
[64] F. Su, S. Ozev, and K. Chakrabarty, "Test planning and test resource optimization for droplet-based microfluidic systems," *J. Electron. Test.: Theory Appl.*, vol. 22, no. 2, pp. 199–210, 2006.
[65] F. Su and K. Chakrabarty, "Module placement for fault-tolerant microfluidics-based biochips," *ACM Trans. Design Automat. Electron. Syst.*, vol. 11, no. 3, pp. 682–710, 2006.
[66] F. Su and K. Chakrabarty, "High-level synthesis of digital microfluidic biochips," *ACM J. Emerg. Technologies in Computing Systems*, vol. 3, no. 4, 2008.
[67] F. Su, "Synthesis, testing, and reconfiguration techniques for digital microfluidic biochips," Ph.D. dissertation, Dept. Elect. Comput. Eng., Duke Univ., Durham, NC, 2006.
[68] T. Xu and K. Chakrabarty, "Droplet-trace-based array partitioning and a pin assignment algorithm for the automated design of digital microfluidic biochips," in *Proc. IEEE/ACM Int. Conf. Hardw./Softw. Codesign Syst. Synth.*, 2006, pp. 112–117.
[69] T. Xu and K. Chakrabarty, "Functional testing of digital microfluidic biochips," in *Proc. IEEE Int. Test Conf.*, 2007, pp. 1–10.
[70] T. Xu and K. Chakrabarty, "Parallel scan-like test and multiple-defect diagnosis for digital microfluidic biochips," *IEEE Trans. Biomed. Circuits Syst.*, vol. 1, no. 2, pp. 148–158, Jun. 2007.
[71] T. Xu and K. Chakrabarty, "Integrated droplet routing in the synthesis of microfluidic biochips," in *Proc. IEEE/ACM Design Automat. Conf.*, 2007, pp. 948–953.
[72] T. Xu and K. Chakrabarty, "A cross-referencing-based droplet manipulation method for high-throughput and pin-constrained digital microfluidic arrays," in *Proc. DATE Conf.*, 2007, pp. 552–557.
[73] T. Xu and K. Chakrabarty, "Broadcast electrode-addressing for pin-constrained multi-functional digital microfluidic biochips," in *Proc. IEEE/ACM Design Automat. Conf.*, 2008, pp. 173–178.
[74] P.-H. Yuh, C.-L. Yang, and Y.-W. Chang, "Placement of defect-tolerant digital microfluidic biochips using the T-tree formulation," *ACM J. Emerg. Tech. Comput. Sys.*, vol. 3, no. 3, pp. 13.1–13.32, 2007.
[75] P.-H. Yuh, C.-L. Yang, and Y.-W. Chang, "BioRoute: A network flow based routing algorithm for digital microfluidic biochips," in *Proc. ICCAD*, 2007, pp. 752–757.
[76] P.-H. Yuh, S. Sapatnekar, C.-L. Yang, and Y.-W. Chang, "A progressive-ILP based routing algorithm for cross-referencing biochips," in *Proc. DAC*, 2008, pp. 284–289.
[77] M. Cho and D. Z. Pan, "A high-performance droplet router for digital microfluidic biochips," in *Proc. ISPD*, 2008, pp. 200–206.
[78] S.-K. Fan, C. Hashi, and C.-J. Kim, "Manipulation of multiple droplets on $N \times M$ grid by cross-reference EWOD driving scheme and pressure-contact packaging," in *Proc. MEMS*, 2003, pp. 694–697.
[79] H. Brenner and D. Edwards, *Macrotransport Processes* (Butterworth-Heinemann Series in Chemical Engineering). Boston, MA: Butterworth-Heinemann, 1993.
[80] *"Benchmarks" for Digital Microfluidic Biochip Design and Synthesis* [Online]. Available: http://people.ee.duke.edu/∼fs/Benchmark.pdf
[81] K. Chakrabarty, "Design automation and test solutions for digital microfluidic biochips," *IEEE Trans. Circuits Syst. I*, vol. 57, no. 1, pp. 4–17, Jan. 2010.

Krishnendu Chakrabarty (F'08) received the B.Tech. degree from the Indian Institute of Technology Kharagpur, Kharagpur, India, in 1990, and the M.S.E. and Ph.D. degrees from the University of Michigan, Ann Arbor, in 1992 and 1995, respectively.

He is currently a Professor of Electrical and Computer Engineering with Duke University, Durham, NC. He is also a member of the Chair Professor Group (honorary position) in Software Theory at the School of Software, Tsinghua University, Beijing, China. His current research interests include testing and design-for-testability of integrated circuits, digital microfluidics and biochips, circuits and systems based on DNA self-assembly, and wireless sensor networks. He has authored nine books on these topics, published over 330 papers in journals and refereed conference proceedings, and given over 130 invited, keynote, and plenary talks.

Dr. Chakrabarty is a recipient of the National Science Foundation Early Faculty (CAREER) Award, the Office of Naval Research Young Investigator Award, the Humboldt Research Fellowship from the Alexander von Humboldt Foundation, Germany, and several best papers awards at IEEE conferences. He is also a recipient of the 2008 Duke University Graduate School Dean's Award for excellence in mentoring, and the Pratt School of Engineering's 2010 Capers and Marion McDonald Award for Excellence in mentoring and advising. He has served as a Distinguished Visitor of the IEEE Computer Society from 2005 to 2007, and as a Distinguished Lecturer of the IEEE Circuits and Systems Society from 2006 to 2007. Currently, he serves as an ACM Distinguished Speaker and a Distinguished Visitor of the IEEE Computer Society for 2010–2012. He is an Associate Editor of the IEEE TRANSACTIONS ON COMPUTER-AIDED DESIGN OF INTEGRATED CIRCUITS AND SYSTEMS, IEEE TRANSACTIONS ON CIRCUITS AND SYSTEMS II, and IEEE TRANSACTIONS ON BIOMEDICAL CIRCUITS AND SYSTEMS. He also serves as an Editor of the *Journal of Electronic Testing: Theory and Applications*. He is the Editor-in-Chief for the IEEE DESIGN AND TEST OF COMPUTERS, and *ACM Journal on Emerging Technologies in Computing Systems*. He is a Golden

Core Member of the IEEE Computer Society, and a Distinguished Engineer of ACM. He was a 2009 Invitational Fellow of the Japan Society for the Promotion of Science.

Richard B. Fair (LF'09) received the Ph.D. degree from Duke University, Durham, NC, in 1969.

He was with Bell Laboratory, Murray Hill, NJ, for 12 years, working on semiconductor devices and integrated circuit technology. He was involved in the research, development and manufacturing of semiconductor devices and had direct experience with the manufacture, design, and testing of metal-oxide-semiconductor (MOS) dynamic memory chips. He also performed research and development in power MOS and bipolar transistors and power Schottky diodes for use in low-power-loss switch mode power converters. He returned to North Carolina in 1981 and spent 13 years as a Vice President of Microelectronics Corporation of North Carolina, Research Triangle Park, having responsibilities in chip design, computer-aided design, packaging, materials, and process technology. He is currently the Lord-Chandran Professor of Engineering with Duke University. He currently teaches electrical engineering courses in semiconductor devices, semiconductor processing, integrated circuit design, and biochip engineering. He has published over 150 papers in refereed journals and conference proceedings, authored 11 book chapters, edited nine books or conference proceedings, and given over 120 invited talks, mostly in the area of semiconductor devices or the fabrication thereof.

Dr. Fair is a Fellow of the Electrochemical Society. He was the Editor-in-Chief of the PROCEEDINGS OF THE IEEE, and has served as an Associate Editor of the IEEE TRANSACTIONS ON ELECTRON DEVICES. He was a recipient of the IEEE Third Millennium Medal in 2000, and the 2003 Solid State Science and Technology Prize and Medal from the Electrochemical Society, which was presented in Paris.

Jun Zeng (M'09) received the B.S. degree from the University of Science and Technology of China, Hefei, China, and the M.S. and Ph.D. degrees from Johns Hopkins University, Baltimore, MD.

He is currently a Senior Researcher with Hewlett-Packard Laboratories, Hewlett-Packard Company, Palo Alto, CA. He is also a term ad hoc Faculty Member with Duke University's Graduate School, Durham, NC, and a Ph.D. Thesis Committee Member in the Department of Electrical and Computer Engineering. His publications include 40 peer-reviewed papers and he has co-edited a book on computer-aided design of integrated systems.

Dr. Zeng has served as a Guest Editor of the IEEE TRANSACTIONS ON COMPUTER-AIDED DESIGN OF INTEGRATED CIRCUITS AND SYSTEMS. He is a proposal reviewer for the National Science Foundation, and a reviewer for several scientific journals. He is a member of the Advisory Board on Hewlett-Packard Laboratories' Open Innovation Research Grants.